Computer Standards & Interfaces 70 (2020) 103417

Contents lists available at ScienceDirect

Computer Standards & Interfaces

journal homepage: www.elsevier.com/locate/csi

The impact of error control schemes on lifetime of energy harvesting wireless sensor networks in industrial environments

Nazli Tekin*, Vehbi Cagri Gungor

Department of Computer Engineering, Abdullah Gul University, Kayseri, Turkey

ARTICLE INFO

Keywords:
Error control
Energy harvesting
Network lifetime
Industrial wireless sensor networks

ABSTRACT

Due to the harsh channel conditions of the industrial environments, the data transmission over the wireless channel suffers from erroneous packets. The energy consumption of error control schemes is of great importance for battery-limited Wireless Sensor Networks (WSNs) in industrial environments. In this paper, the lifetime analysis of error control schemes, i.e., Automatic Repeat Request (ARQ), Forward Error Correction (FEC) and Hybrid ARQ (HARQ), is presented under different industrial environment channel conditions. Furthermore, the impact of energy harvesting methods on the network lifetime is investigated. A novel Mixed Integer Programming (MIP) framework is developed to maximize the network lifetime while meeting application reliability. Performance results show that utilizing HARQ-II error control scheme for Mica2 and BCH(31,21,5) for Telos improves the network lifetime while meeting the desired application reliability rate.

1. Introduction

Recently, wireless sensor networks (WSNs) in industrial environments have gained great interest due to the expanding diversity of their applications [1,2]. In real-time process control applications, wireless sensor nodes are deployed in factories to acquire data for preventing any trouble in operations by early notifications [3]. In addition to process control applications, maintenance applications monitor the health of equipment periodically to recognize unexpected changes and thus, to avoid from high repair expenses and delays caused by the temporary failures of machine working. Furthermore, industrial mobile robots move around machines to monitor the environment and calibrate the deployed sensor nodes. Moreover, the industrial environment monitoring applications alert managers if there is any emergency, including leakage of flammable liquids or gases. With the advantages of WSNs, industrial applications have gained self-configuration and self-organizing characteristics [4,5].

Besides many advantages of WSNs, low power communication constraints of sensor nodes induce packet drops and erroneous packet deliveries over wireless links [6]. Since noises and RF interference on the wireless channel may endanger the reliable communication, utilizing the error detection and correction techniques becomes essential to improve the link reliability [7]. However, providing the reliability causes substantial energy costs on WSNS due to packet retransmissions or overhead of error control schemes. To this end, Energy Harvesting (EH) methods provide a viable solution for the battery-powered industrial sensor nodes to improve the network lifetime. Energy can be harvested from the various ambient resources and the industrial environments utilizing solar, thermal vibration harvesters [3].

To address these challenges, in this paper, we have evaluated the performance of Automatic Repeat Request (ARQ), a Forward Error Control (FEC) and Hybrid ARQ (HARQ) schemes in terms of energy consumption while achieving the desired application reliability in industrial environments. We also consider the indoor solar, thermal and vibration based harvester to scavenge energy from the industrial environments and evaluate their impacts on the network lifetime. Importantly, we have proposed the Mixed Integer Programming (MIP) model considering the impacts of both energy harvesting and error control approaches to maximize the network lifetime in industrial environments while meeting application reliability.

To summarize, the main contributions of this study are as follows:

- The impact of exploiting error control schemes, such as ARQ, FEC (*i.e.*, BCH(31,11,5), BCH(31,21,5), RS(15,11,5)) and HARQ (*i.e.*, HARQ-I, HARQ-II) on industrial wireless network lifetime is investigated while meeting desired application reliability. The performance evaluations have been conducted based on the power consumption characteristics of Mica2 and Telos motes.
- The impact of energy harvesting methods, which are indoor solar, thermal and vibration-based harvesters, on industrial network

* Corresponding author.
E-mail addresses: nazli.tekin@agu.edu.tr (N. Tekin), cagri.gungor@agu.edu.tr (V.C. Gungor).

https://doi.org/10.1016/j.csi.2020.103417
Received 4 April 2019; Received in revised form 6 January 2020; Accepted 6 January 2020
Available online 09 January 2020

Table 1
Literature overview.

Paper	Industrial channel model	Error control	Network lifetme analysis	Energy harvesting	Application relability	Hardware character
[8–10]	✗	✓	✗	✗	✗	**Mica2, MicaZ**
[11]	✗	✓	✗	✗	✓	**MicaZ**
[12,13]	✓	✓	✗	✗	✗	**MicaZ**
[14]	✗	✓	✗	✓	✗	**MicaZ**
[15]	✗	✓	✗	✗	✗	✗
[16]	✓	✓	✗	✓	✗	✗
[17,18]	✗	✓	✗	✓	✗	✗
Proposed system	✓	✓	✓	✓	✓	**Mica2, Telos**

lifetime is examined.

- The realistic wireless channel model of industrial environment is employed. To this respect, log normal shadowing model is utilized to consider path loss characteristics and error rates on the industrial propagation environments.
- The MIP framework with the objective of maximizing the network lifetime in industrial environments is formulated while jointly considering realistic channel and energy dissipation models, the error control schemes and energy harvesting methods.

The rest of the paper is organized as follows. Section 2 presents the previous work on error control and energy harvesting approaches. Section 3 elaborates the system model. Section 4 presents the performance results. Finally, Section 5 concludes the paper.

2. Related ork

In the literature, there are several studies [8,9] focusing on analysis of error control schemes in terms of energy efficiency and reliability in WSNs. For instance, Vuran et. al [8] have studied the cross layer analysis of error control schemes by considering routing, Medium Access Control (MAC) and physical layers. In this analysis, they have compared the FEC, ARQ and HARQ in terms of energy consumption, latency and Packet Error Rate (PER). Nandi and Kundu [9] have investigated the error control schemes in terms of energy consumption and optimum error correcting capability by taking account of Rayleigh fading. As a result they have shown that FEC schemes enhance energy efficiency compared to ARQ by optimizing correcting capability and the PER performance of FEC schemes is better than the ARQ. Islam [10] investigates the suitable error correction codes in wireless sensor network by taking into account of Bit Error Rate (BER) and power consumption. Naderi et. al [11] have evaluated the performance of error control schemes for real-time multimedia communication. They have analyzed the cumulative jitter and frame loss rate in multimedia communication considering tradeoff between the energy efficiency and reliability. Sarvi et. al [12] have introduced a new adaptive cross layer error control protocol (NAC) for multimedia wireless sensor networks. The proposed method dynamically changes the redundancy bits according to packet loss rate. Razali et. al [13] have evaluated existing error control schemes in terms of bit length and proposed HARQ error control algorithm.

In addition, numerous studies have utilized the energy harvesting to increase energy level of batteries while investigating the error control schemes. Jalali et. al [14] have considered the solar energy harvester to recharge battery of sensor nodes in their studies. They have worked on Cooperative ARQ (CARQ), which distributes the energy consumption among sensor nodes in energy harvesting WSN. In CARQ scheme, when retransmission is necessary, cooperator node resends the data instead of source node to reduce the energy consumption of source node. Sharma et.al [15] have evaluated the Packet Drop Probability (PDR) of energy harvesting sensor nodes which apply either an ARQ protocol or HARQ with chase combining (HARQ-CC) protocol by considering slow and fast channel fading. They have shown the effect of energy harvesting rate on the sensor nodes performance. Mahdavi et. al [16] have investigated the throughput performance of Repetititon-HARQ and Incremental Redundancy HARQ (IR-HARQ) by using sensor nodes, which harvest energy at receiver nodes only. To decrease processing energy consumption, receiver nodes scavenge energy with the limited harvesting rate. They have presented that Repetition-HARQ performs better than IR-HARQ in terms of energy constraints. Yadav et. al [17] have proposed the adaptive ARQ based error control scheme for energy harvesting sensor nodes. They consider the sensor nodes harvesting energy with a fixed rate at a time. They have shown that the proposed method gives better results over the conventional schemes. Many of the above mentioned papers have implemented energy harvesting by assuming constant harvesting rates. However in our study, we apply realistic energy harvesting methods used in industrial environments.

Jung et. al [18] have proposed the adaptive FEC protocol to enhance the data reliability. Since Reed Solomon code has been the most efficient one, they have developed energy-aware Reed Solomon (EA-RS) method. According to residual energy of sensor nodes, the method adjusts the length of parity bits. If residual energy is high enough, sensor node sends data with long parity bits to ensure reliability. If residual energy is not high enough, sensor node transmits data with short parity bits to decrease the energy consumption.

An overview of the various approaches that focus on energy consumption of the error control schemes and present energy-aware protocols is illustrated in Table 1. All these studies provide valuable insights about wireless sensor network's lifetime and reliability. However, none of them focus on the impact of error control schemes on network lifetime in industrial environments. In our previous study [19], we have evaluated the effect of error control schemes on network lifetime in industrial environments. The objective of this paper is to extend the study further by proposing the Mixed Integer Programming (MIP) model considering the impacts of both energy harvesting and error control approaches to maximize the network lifetime in industrial environments while meeting application reliability.

3. System model

In this section, we present the physical layer model, link layer model, energy harvesting model and MIP model that we consider in our performance evaluations. The network lifetime is defined as the time until the first node depletes its all battery energy. Additionally, we define application reliability rate as the ratio of data received by the sink node to data generated by all sensors in the network. To this end, the rate of application reliability is shown as

$$Reliability = \frac{DataPacket_{Sink}^{Received}}{\sum_{i \in W} DataPacket_{i}^{Generated}}, \quad (1)$$

where W is the set of sensor node in the network.

We also define the normalized lifetime in order to compare network lifetime while exploiting various error control schemes for Mica2 and Telos. The normalized lifetime is obtained by dividing absolute lifetime minus minimum lifetime to the maximum lifetime value shown as below

$$NormalizedLifetime = \frac{Lifetime_{abs} - Lifetime_{min}}{Lifetime_{max}}. \quad (2)$$

In addition, the lifetime improvement is defined to show the effect of energy harvesting methods on the network lifetime. The lifetime improvement (LI) is calculated as lifetime with energy harvesting minus lifetime without energy harvesting divided by lifetime without energy harvesting as follows

$$LI = \frac{Lifetime_{withEH} - Lifetime_{withoutEH}}{Lifetime_{withoutEH}} \times 100. \quad (3)$$

3.1. Physical layer model

In industrial propagation environments, the signal strength may be affected due to noise, RF interference, signal diffraction, reflection and scattering. In this study, the four different topographies are defined on the basis of RF propagation characteristics of the indoor industrial environments [20]:

- **L**ine of Sight (LOS): Signals along the path can propagate between transmitter and receiver. In other words, line of sight between transmitting and receiving antenna exists along the path.
- **O**bstructed Path (OBS) with light clutter: Such paths exist when a LOS path is blocked partially by and industrial machinery or obstruction.
- **O**bstructed Path (OBS) with heavy clutter: The industrial machine blocks the transmitter and receiver along the aisles. Such a radio path would typically exist across aisles in a stocked warehouse.
- **A**LL LSF topographies: The integration of the above three topographies.

In this paper, we utilize the log normal shadowing model to better represent the path loss and shadowing deviation on industrial environments [21]. The path loss, $PL_{ij}(d)$, over link between node i and node j for this model is given by

$$PL_{ij}(d) = PL(d_0) + 10n \log_{10}\left(\frac{d_{ij}}{d_0}\right) + X_\sigma, \quad (4)$$

where d_{ij} and d_0 represents the transmission distance between node i and node j and the reference distance, respectively. n denotes the path loss exponent, and X_σ indicates a Gaussian random variable (in dB) with zero mean and σ standard deviation. Also, $PL(d_0)$ symbolizes the path loss in reference distance. Signal-to-noise ratio (SNR) γ_{ij} at distance d_{ij} is computed as:

$$\gamma_{ij} = P_t - PL_{ij}(d_{ij}) - P_n, \quad (5)$$

where P_t is the output power and P_n is the noise floor. Since FSK is implemented as a modulation scheme in Mica2 motes [8], the Bit Error Rate (BER) is calculated by

$$P_{b,ij}^{FSK} = \frac{1}{2}\exp^{-\frac{E_b/N_0}{2}}, \quad (6)$$

where

$$E_b/N_0 = \gamma\frac{B_N}{R}, \quad (7)$$

where γ is the received SNR, B_N is the noise bandwidth, and R is the data rate. For Mica2 motes, R= is 19.2 kbps and B_N= is 30 kHz. The probability of successfully transmitting a packet from node i to node j, p_{ij}^s, is given by [22]

$$p_{ij}^s(q) = (1 - \frac{1}{2}\exp^{-\frac{\gamma_{ij}}{2}\frac{1}{0.64}})^{8q}, \quad (8)$$

where q is the packet size. Since Telos mote is implemented with O-QPSK modulation the BER is calculated by

$$P_{b,ij}^{O-QPSK} = Q(\sqrt{(E_b/N_0)_{DS}}), \quad (9)$$

where

$$(E_b/N_0)_{DS} = \frac{2NE_b/N_0}{N + 4E_b/N_0(K-1)/3}. \quad (10)$$

In Eq. (10), N is the number of chips per bit and K is the number of simultaneous users. Therefore, the probability of successfully transmitting a packet from node i to node j, p_{ij}^s, is given by

$$p_{ij}^s(q) = (1 - Q(\sqrt{(E_b/N_0)_{DS}}))^{8q}. \quad (11)$$

For ARQ, the probability of packet failure p_{ij}^f which is also called Packet Error Rate(PER) is calculated as folows:

$$p_{ij}^f(q) = 1 - p_{ij}^s(q). \quad (12)$$

FEC block code is represented by (n,k,t) where n is the block length, k is the payload length and t is the error correcting capability. The Block Error Rate (BLER) is shown by

$$BLER_{ij}(n, k, t) = \sum_{l=t+1}^{n} \binom{n}{l} P_{b,ij}^l (1 - P_{b,ij})^{n-l}. \quad (13)$$

The PER for BCH and RS is defined as in [23]:

$$PER(q, n, k, t) = 1 - (1 - BLER(n, k, t))^{\lceil \frac{q}{k} \rceil}, \quad (14)$$

where $\lceil \frac{q}{k} \rceil$ is the number of blocks required to send q bits.

3.2. Link layer model

Error Control schemes in WSNs are basically classified into three main approaches that are ARQ, FEC and HARQ:

- **Automatic Repeat Request (ARQ):** To recover the lost data packets, ARQ schemes utilize the retransmissions of data packets. Receiver informs transmitter with acknowledgement (ACK) packet if there is an erroneous or lost packet. It is obvious that the retransmission mechanisms of ARQ schemes impose the significant amount of energy cost on the sensor node.
- **Forward Error Correction (FEC):** The redundant bits are added to the transmitted data packets in FEC schemes. Receiver node corrects the errors on the data packets by using these redundant bits. Apparently, the redundant bits lead to additional energy cost for both transmitter and receiver. In addition, receiver also incurs the decoding energy cost. There are different FEC schemes optimized for specific conditions and requirements. Since they are energy efficient for WSNs, we have analyzed Bose Chaudhuri Hocquenghem (BCH) and Reed Solomon (RS) FEC codes in our study. FEC codes represented by (n,k,t) divide a packet into n blocks of group to encode before transmitting. Here, k refers the payload length on these blocks and t is the number of bits that FEC code can correct.
- **Hybrid ARQ (HARQ):** HARQ combines ARQ along with FEC codes. There are two types of schemes which are HARQ-I and HARQ-II. In HARQ-I, transmitter sends the data packet and waits for and acknowledgement. If NACK received, transmitter resends the data encoded with FEC code. In HARQ-II, transmitter sends the data packet and if received NACK packet, it will resend only the redundant bits.

3.2.1. Communication energy calculations

For ARQ, the transmission energy includes sending data, receiving acknowledgement and retransmission costs [23]. Therefore, the amount of energy consumed by node i for successfully transmitting L_P bits data packet to node j can be expressed as follows:

$$E_{tx,ij}^{ARQ} = E_{enc} + n_{ret,ij}^{ARQ}\{(E_{tx}(L_P) + E_{rx}(L_A)) + E_{to}\}. \quad (15)$$

The amount of energy consumed by node j for receiving the data and

Maximize H
Subject to:

$$f_{ij} \geq 0, \forall (i,j) \in A \tag{43}$$

$$f_{1j} = 0, \forall (j) \in W \tag{44}$$

$$\sum_{(i,j)\in A} f_{ij} - \sum_{(j,i)\in A} f_{ji} \times \phi_{ji} = H \times s, \forall i \in W \tag{45}$$

$$\sum_{(j,1)\in A} f_{j1} \times \phi_{j,1} \geq \sum_{j\in W} s \times H \times r \tag{46}$$

$$T_{busy,i} = \sum_{i\in W} T_{tx,ij} \times f_{ij} \times n_{ret,ij} + \sum_{i\in W} T_{rx} \times f_{ji} \times n_{ret,ji} + H \times T_{acq}, \forall i \in W \tag{47}$$

$$\sum_{j\in W} E_{tx,ij} \times f_{ij} + \sum_{j\in W} E_{rx,ji} \times f_{ji} + (H \times E_{acq}) + P_{slp} \times (H \times T_{rnd} - T_{busy,i}) - P_{harv} \times (H \times T_{rnd} - T_{busy,i}) \leq \xi, \forall i \in W \tag{48}$$

$$(L_P + L_A) \times \sum_{j\in W} f_{ij} \times n_{ret,ij} + \sum_{j\in W} f_{ji} \times n_{ret,ji} \leq \varsigma \times H \times T_{rnd} \forall i \in V \tag{49}$$

Fig. 1. The MIP framework that maximizes network lifetime.

replying with an ACK packet is determined by

$$E_{rx}^{ARQ} = n_{ret,ij}^{ARQ} \times (E_{rx}(L_P) + E_{tx}(L_A)), \tag{16}$$

where $E_{tx}(x)$, $E_{rx}(x)$ are the energy consumed for the packet transmission and reception and are explained in Eq. (23). L_P and L_A refer to the length of data and acknowledgement packets, respectively. E_{to} is the energy consumed by node i before timeout which includes propagation delay plus guard time and formulated by

$$E_{to} = P_{std} \times (T_{pd} + T_{grd}), \tag{17}$$

where P_{std} is standby power. T_{pd} and T_{grd} are propagation delay defined as the time that data travel from source to destination and guard time which is the tame waiting for acknowledgement. The probability of successful handshake communication (transmit data and receive acknowledgement) can be considered as follows [24]:

$$p_{ij}^{HS,s} = p_{ij}^{s}(L_P) \times p_{ji}^{s}(L_A). \tag{18}$$

The number of retransmission is calculated by

$$n_{ret,ij} = \frac{1}{p_{ij}^{HS,s}}. \tag{19}$$

The packet success rate after the finite number of retransmission is determined by [25]

$$\phi_{ij} = 1 - [1 - p_{ij}^{HS,s}]^{(n_{ret,ij}+1)}. \tag{20}$$

For FEC, the amount of transmission energy is given as follows:

Table 2
Simulation parameters for energy harvesters.

Indoor solar harvester			
Sy/Ac/Vr	**Description**	**Unit**	**Value**
T_C	Ambient temperature	K	295
n	Number of PV cells	–	15
I_0	Current of p-n nodes	A	1×10^{-9}
I_{SC}	Current of light irradiance	\muA	150
q	Charge of electron	C	1.6022×10^{-19}
k	Boltzmans constant	JK^{-1}	1.3807×10^{-23}
Thermal harvester			
Sy/Ac/Vr	**Description**	**Unit**	**Value**
ΔT	Temperature differences	K	10
n	Number of thermocouples	–	5200
α	Seebeck's coefficients	mV/K	0.21
R_s	Electrical resistance	$k\Omega$	82
Vibration harvester			
Sy/Ac/Vr	**Description**	**Unit**	**Value**
ω	Frequency	Hz	71
V	Voltage	V	48
I	Current	mA	0.05

Table 3
Average harvested power.

Harvester	Unit	Value
Indoor solar	mW	0.4947
Thermal	mW	0.3635
Vibration	mW	0.2400

Table 4
The channel parameters.

Topography	n	σ
LOS	2.40	4.79
OBS (light clutter)	2.77	5.42
OBS (heavy clutter)	4.29	8.42
ALL LSF	3.44	8.63

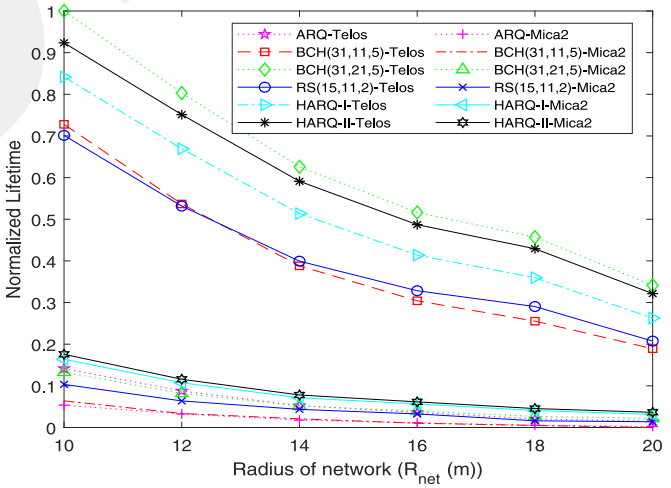

Fig. 2. Normalized lifetime with various radius of network (R_{net} (m)) for Mica2 and Telos.

$$E_{tx,ij}^{FEC} = E_{enc} + E_{tx}(L_P). \tag{21}$$

The receiver (node j) consumes energy for receiving a data packet and decoding. Thus, the reception energy is given by

$$E_{rx,ij}^{FEC} = (E_{rx}(L_P) + E_{dec}(L_P)). \tag{22}$$

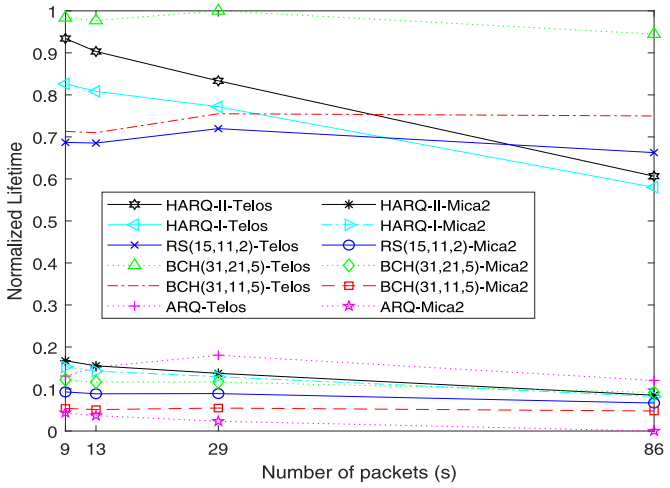

Fig. 3. Normalized lifetime with various number of packets (s) for Mica2 and Telos.

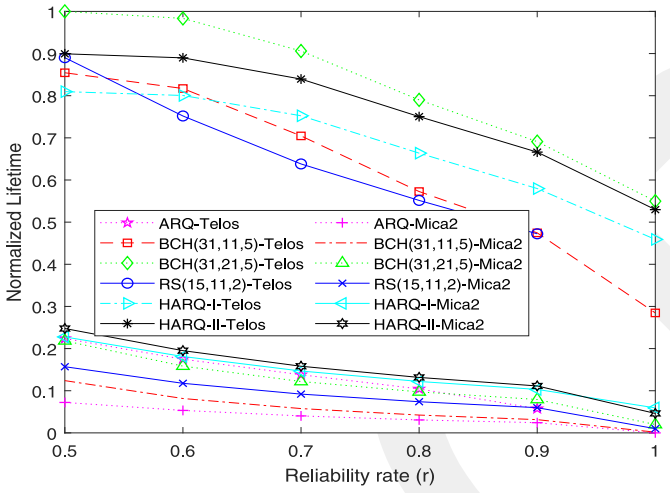

Fig. 4. Normalized lifetime with various reliability rate (r) for Mica2 and Telos.

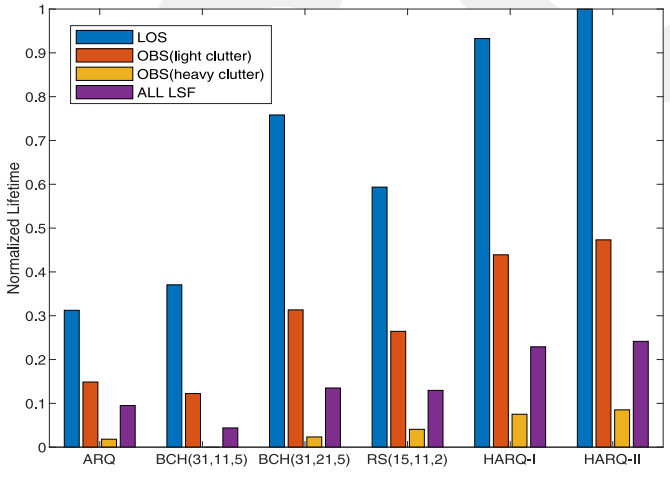

Fig. 5. Normalized lifetime with different topographies for Mica2 .

$E_{tx}(x)$ and $E_{rx}(x)$ are shown below

$$E_{tx}(x) = E_{elec} + P_t(\tfrac{x}{R})$$
$$E_{rx}(x) = E_{elec} + P_r(\tfrac{x}{R}), \tag{23}$$

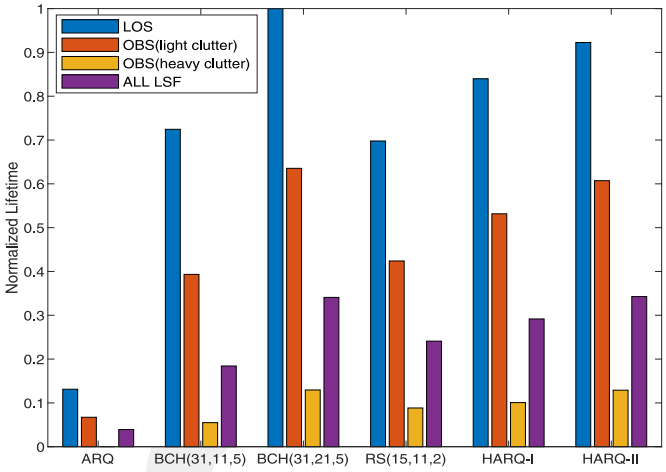

Fig. 6. Normalized lifetime with different topographies for Telos.

where E_{elec} refers to energy per bit needed by transmitter electronics. R denotes the data rate. $E_{dec}(L_P)$ refers to the energy consumption for decoding the FEC code and is given by

$$E_{dec}(L_P) = P_{proc}T_{dec}(L_P) \tag{24}$$

where P_{proc} is processing power and T_{dec} is given in section (3.2.2). Here, it is important to note that only the decoding energy is evaluated since the encoding energy (E_{enc}) is negligibly small [26].

For HARQ, transmitter (node i) sends a data packet first with ARQ and if replied with NACK, the transmitter resends the data packet using FEC scheme. Hence, the transmission energy is given as follows:

$$E_{tx,ij}^{HARQ} = E_{enc} + E_{tx}(L_{P_f}) + (1 - p_{ij}^{s}(L_{P_f}))(E_{rx}(L_{P_n}) + E_{tx}(L_{P_s})), \tag{25}$$

where L_{P_f} and L_{P_s} refer to the packets for the first and second transmitted packets, respectively. $p_{ij}^{s}(L_{P_f})$ denotes the probability that the first data packet is successfully received at a distance d(i, j) and the (L_{P_n} is the size of the NACK packet. The reception energy is given as

$$E_{rx,ij}^{HARQ} = E_{rx}(L_{P_f}) + E_{dec}(L_{P_f}) + (1 - p_{ij}^{s}(L_{P_f}))(E_{tx}(L_{P_n}) + E_{rx}(L_{P_s}) + E_{dec}(L_{P_s})). \tag{26}$$

3.2.2. Latency analysis

For ARQ, the time spending for transmitting a data packet from node i to node j and waiting for ACK is given by

$$T_{tx,ij}^{ARQ} = \frac{L_P}{R} + T_{pd} + T_{grd}. \tag{27}$$

Time spending for receiving a data packet in ARQ is given by

$$T_{rx,ij}^{ARQ} = \frac{L_P}{R}. \tag{28}$$

For FEC, time spending for transmitting a data packet is given by

$$T_{tx,ij}^{FEC} = \frac{L_P}{R} + T_{pd}. \tag{29}$$

Time spending for receiving a data packet in FEC and decoding data is given by

$$T_{rx,ij}^{FEC} = \frac{L_P}{R} + T_{dec}. \tag{30}$$

$T_{dec,bc}$ refers to decoding time for the FEC block code (n,k,t), and it is expressed as follows:

$$T_{dec,bc} = (2nt + 2t^2) \times (T_{add} + T_{mult}), \tag{31}$$

where T_{add} and T_{mult} are the time period for addition and multiplication,

Table 5
Lifetime improvement of various energy harvesters.

		Lifetime improvement (%)					
		Mica2					
		ARQ	BCH(31,11,5)	BCH(31,21,5)	RS(15,11,5)	HARQ-I	HARQ-II
	Vibration	5.6	6	13	10	16	18
	Thermal	7	10	21	16	27	30
$R_{net=10}$ (m)	Indoor Solar	12	14	32	24	41	46
	Vibration	3.5	4	8	7	10	11
	Thermal	5	5	13	10	17	18
$R_{net=12}$ (m)	Indoor Solar	7	7	18	15	25	27
	Vibration	2	2	6	4	7	8
	Thermal	3	3.4	9	7	8	9
$R_{net=14}$ (m)	Indoor Solar	4	5	12	10	16	18
	Vibration	1.3	1.3	4	3	5	6
	Thermal	2	2	6	5	8	9
$R_{net=16}$ (m)	Indoor Solar	3	3	9	7	11	13
	Vibration	1	0.8	3	2	4	4
	Thermal	1.5	1.2	4	3	6	6
$R_{net=18}$ (m)	Indoor Solar	2	1.7	6	4	8	9
	Vibration	0.5	0.3	2	1.3	2.7	3
	Thermal	0.8	0.4	3	2	4	5
$R_{net=20}$ (m)	Indoor Solar	1	0.6	4	3	6	7
		Telos					
		ARQ	BCH,(31,11,5)	BCH(31,21,5)	RS(15,11,5)	HARQ-I	HARQ-II
	Vibration	4	18	25	17	20	23
	Thermal	6	29	44	28	35	39
$R_{net=10}$ (m)	Indoor Solar	8	45	71	43	54	62
	Vibration	3	13	20	13	16	18
	Thermal	4	21	33	21	26	30
$R_{net=12}$ (m)	Indoor Solar	7	31	52	30	40	46
	Vibration	2	9	15	10	12	14
	Thermal	3	15	24	15	19	23
$R_{net=14}$ (m)	Indoor Solar	4	21	37	22	29	34
	Vibration	1.5	7	12	8	10	11
	Thermal	2	11	20	12	15	18
$R_{net=16}$ (m)	Indoor Solar	3	16	29	17	22	26
	Vibration	1	6	11	7	8	10
	Thermal	1.5	9	17	11	13	16
R_{net} = 18 (m)	Indoor Solar	2	13	24	16	19	23
	Vibration	0.8	4	8	5	6	7
	Thermal	1.3	7	12	7	9	11
R_{net} = 20 (m)	Indoor Solar	1.7	9	17	10	13	16

respectively, of field elements in $GF(2m)$, $m = \lfloor log2n + 1 \rfloor$ [27]. As Mica2 nodes are implemented with 8-bit micro-controllers, which can perform addition and multiplication of 8 bits in 1 and 2 cycles, respectively t is 8. For Telos nodes with 16-bit micro-controllers, t is 16. As a result

$$T_{add} + T_{mult} = 3\frac{m}{t}t_{cycle}, \tag{32}$$

where t_{cycle} is duration of one cycle. Finally, time period of decoding a packet is

$$T_{dec}(L_P) = T_{dec,bc}[\frac{L_P}{k}], \tag{33}$$

where $[\frac{L_P}{k}]$ is the number of block required to send L_P bits. For HARQ, the time spending for transmitting a data packet is given by

$$T_{tx,ij}^{HARQ} = T_{tx,ij}^{ARQ} + T_{tx,ij}^{FEC}. \tag{34}$$

For HARQ, time spending for receiving a data packet is given by

$$T_{rx,ij}^{HARQ} = T_{rx,ij}^{ARQ} + T_{rx,ij}^{FEC}. \tag{35}$$

3.3. Energy harvesting model

Energy harvesting is the process that gathers different kinds of energy from environment (e.g. solar) or from ambient sources (e.g. vibration) and converts it into electricity [28]. In this paper, we focus on indoor solar, thermal, and vibration-based energy harvesters which are available in industrial environments.

3.3.1. Indoor solar harvester

Artificial lights are used as a source for industrial environment harvesters. Photovoltaic cells are utilized to convert light energy to electrical energy [29]. The current of photovoltaic (PV) cells is estimated by

$$I_{PV} = I_L - I_0[\exp(\frac{V_{PV} + I_{PV}R_s}{n_s V_t}) - 1]. \tag{36}$$

In (36), I_L represents the light generated current (A), I_0 denotes the reverse saturation current of the p-n diodes,R_s indicates the series resistance of the cells (Ω) and V_t is the thermal voltage of the cells and can be calculated using:

$$V_t = \frac{kT_c}{q}, \tag{37}$$

where k is the Boltzmanns constant, T_c is the cell temperature (K), and q is the charge of the electrons. The maximum power generated from photovoltaic module is calculated as:

$$P = V_{PV}I_L - V_{PV}I_0[\exp(\frac{V_{PV}}{n_s kT_c/q})]. \tag{38}$$

3.3.2. Indoor thermal energy harvester

A Thermo Electric Generator (TEG) converts thermal energy into electricity by utilizing Seebeck effects [30]. The open-circuit voltage

Table 6
Simulation parameters.

Sy/Ac/Vr	Description	Unit	Value
PL(d_0)	Path loss at distance, d_0[20]	dB	63.57
d_0	Reference distance	m	0.5
P_n	Noise Floor	dBm	−93.0
P_t	Output power	dB	0
q	Frame size	bytes	128
γ_{ij}	Signal to Noise Ratio (SNR) over the link-(i,j)	dB	–
P_b	Bit Error Rate (BER)		–
B_N	Noise bandwidth	kHz	30
R	Data rate [31,32]	kbps	19.2 (Mica2) and 250 (Telos)
H	Number of rounds	–	–
f_{ij}	Number of data packets flowing from node-i to node-j	–	–
s_i	Number of data packets generated at each round	–	–
d_{ij}	Distance from node-i to node-j	m	–
$p_{ij}^{s}(q)$	Probability of successfully receiving q byte packet from node-i to node-j	–	–
p_{ij}^{f}	Probability of packet failure	–	–
P_{tx}	Power consumption for transmission [33]	mW	5
P_{rx}	Power consumption for reception[33]	mW	21 (Mica2) and 69 (Telos)
P_{proc}	Power consumption for processing [27,34]	mW	24 (Mica2) 0.9 (Telos)
P_{slp}	Sleep power [35]	mW	0.3 (Mica2) 0.16 (Telos)
E_{tx}^{x}	Energy consumption of a transmitter for x= ARQ/ FEC/HARQ	J	–
E_{rx}^{x}	Energy consumption of a receiver for ARQ x= ARQ/ FEC/HARQ	J	–
E_{dec}	Energy consumption for decoding FEC code	–	–
E_{acq}	Acquisition energy for sensing data[22]	\muJ	600
E_{elec}	Electronics energy [36]	nJ	50
$n_{ret,ij}$	Number of retransmission over the link-(i,j)	–	–
ϕ_{ij}	The success rate over the link (i,j) [25]	–	–
r	Desired Packet Delivery Ratio (PDR) of network(end to end link)		0.8
$T_{tx,ij}$	Transmission time of transmitting a packet from node-i to node-j	s	–
T_{rx}	Reception time	s	–
T_{rnd}	Turnaround time	s	20
T_{acq}	Acquisition time for sensing data[22]	ms	20
$T_{busy,i}$	Total busy time for node-i		–
t_{cycle}	Cycle duration [27], [32]	ns	250 (Mica2) and 62.5 (Telos)
P_{harv}	Harvesting power generated from industrial environments [29]	mW	-
ξ	Initial energy assigned to sensor nodes	kJ	25
L_P	Payload size	byte	128
L_A	Acknowledgement size	byte	20
N	Data size	byte	1024

(V_{oc}) is generated as a result of temperature differences and is given by

$$V_{oc} = S^{*}\Delta T = n^{*}\alpha(T_H - T_C), \tag{39}$$

where S represents the Seebecks coefficient of TEG and α represents the Seebecks coefficient of thermocouples. n is the number of thermocouples in TEG. T_H and T_C symbolize the high temperature and low temperature, respectively. The electrical current is shown by

$$I_{TEG} = \frac{V_{oc} - V_{TEG}}{R_{s,TEG}}, \tag{40}$$

where $R_{s,TEG}$ stands for internal resistance of TEG. Finally, the power generated from thermal harvester can be expressed as

$$P_{TEG} = V_{TEG} I_{TEG} = \frac{V_{TEG} n\alpha(T_H - T_C) - V_{TEG}^2}{R_{s,TEG}}. \tag{41}$$

3.3.3. Indoor vibration energy harvester

Piezoelectric is used to convert mechanical energy into electrical energy by exploiting vibration. The power generated from vibration harvested is described by

$$|P| = \frac{m\zeta_e A^2}{4\omega\zeta_T^2}, \tag{42}$$

where m is the proof mass attached to piezoelectric cantilever beam, ω is the input frequency and A is the amplitude of acceleration in input vibration. ζ_e is the electrical damping ratio and ζ_T is the combined electrical and mechanical damping ratio ($\zeta_T = \zeta_e + \zeta_m$).

3.4. Mixed integer programming model

The objective of the proposed framework is to maximize network lifetime by determining the optimum routing path to relay data to the sink node. The network lifetime is defined as the time until the first node drains out its battery in the network. However, the major problem of this definition is that premature death of sensor node which is continuously selected as relay node. Thus, the optimization framework aims to balance the energy dissipation of all sensor nodes in the network. The objective function and constraints of our model are presented in Fig. 1.

The network topology is symbolized by directed graph $G = (V, A)$. V denotes the set of sensor nodes include base station and A denotes the link between all node pairs. In addition, W defines a set of sensor nodes without base station (i.e., $W = V \setminus \{1\}$). Each sensor node except the sink generates the same amount of the data packets (s) at each round which is predefined time (T_{rnd}). The generated s number of data packets is determined according to the maximum packet size (L_P). In this study, each sensor node collects N bytes of data at each round to transmit towards the sink. The header size of the packet (L_H) is 12 bytes. Therefore, the number of packets is calculated by $s = \lceil \frac{N}{L_P - L_H} \rceil$. The generated data are conveyed to sink node either with a single hop or a multi hop. We define network lifetime as $H \times T_{rnd}$ where H refers to number of rounds, which increase until the first node depletes its battery in the network. Hence, the lifetime maximization means that to maximize the number of round (H) of the weakest node in the network. To achieve this, relay node selection is to be optimized according to energy dissipation of sensor nodes. The decision variables are described

as follows:

- f_{ij}: The number of packets flowing node i to node j.
- ϕ_{ij}: The packet success rate (rate of successfully transmitted packets from node i to node j) defined in Eq. (20).
- $T_{busy,i}$: Time spent by node i for transmission, reception and acquisition during the lifetime.
- $T_{tx,ij}$: Time spent for transmit a packet from node i to node j calculated for ARQ, FEC and HARQ defined in Eqs. (27), (29) and (34), respectively.
- $n_{ret,ij}$: The number of retransmission from node i to node j defined for ARQ defined in Eq. (19). For FEC and HARQ, it is set to 1.
- $E_{tx,ij}$: The energy consumed for transmit a packet from node i to node j described for ARQ, FEC and HARQ defined in Eqs. (15), (21), (25), respectively.

Eq.(43) specify that all flows (i.e $f_{ij}\ \forall(i,j) \in A$) are non negative. Eq. (44) ensures that there is no flow from sink to other nodes. Eq. (45) represents the flow balancing constraint at each sensor nodes except sink node. The total amount of data generated at node i is equal to number of transmitted packets minus number of received packets. Eq. (46) guarantees that at least r percent of all generated data collected at sink. r is the application reliability rate and determined in Eq. (1) according to need of application. Due to packet losses over the links, every packet generated at each node may not be received by the sink node. For instance, let assume r is set to 0.8 and 100 packets are generated from sensor node during the network lifetime, the equation obligates that the at least 80 packets must be received by the sink node. Sensor node is in active mode while acquiring, transmitting or receiving a data. In equation (47), $T_{busy,i}$ is the total time that a node i is in active mode. In other words, it is the sum of required time for transmission, reception and acquisition of data. Equation (48) states that the energy consumption for acquisition and communication for each node except sink must be smaller than the battery of node. P_{harv} is the harvested energy in sleep mode. Equation (49) ensures that the required bandwidth for transmitting and receiving is limited by channel bandwidth.

4. Performance analysis

In our analysis, we create disk shape connected network topology with various R_{net}. Sensor nodes are deployed within the defined topology randomly. The base station is placed at the center of disk shape network with the coordinate of (0,0). Each node has at least one neighbour node within communication distance to provide connectivity among sensor nodes. The communication distance changes according to channel characteristics of industrial environments. R_{net} varies between 10 m and 20 m with an increment of 2 m. L_P takes values of 128, 96, 48 and 24 byte. Note that according to these selected L_P, the number of generated packets in each round is adjusted as 9, 13, 29, 86, respectively. Moreover, we examine six different values of desired application reliability rate (*i.e.* $r = 0.5, 0.6, 0.7, 0.8, 0.9, 1$). We investigate the four different topographies for industrial environment such as LOS, OBS (light clutter), OBS (heavy clutter) and ALL LSF defined in Section 3.1. The channel parameters for different topographies are listed in Table 4 [20]. The simulation parameters are shown in Table 6.

We use MATLAB for channel model, link layer and energy harvesting model presented in Sections 3.1–3.3, respectively while General Algebraic Modelling System (GAMS) with CPLEX solver for our MIP model presented in Section 3.4. We also obtain our performance results with 100 different trials using 50 sensor nodes and present the average values in figures.

To analyze the contributions of energy harvesting methods on the network lifetime, we utilize indoor solar, vibration and thermal harvesters. Simulation parameters of the harvesters are shown in Table 2. The average harvested power values presented in Table 3 estimated according to calculations in Section 3.3.

The Fig. 2 presents the normalized network lifetime as a function of varying radius of network (R_{net}) for Mica2 and Telos in LOS environment. The application reliability rate (r) is fixed to 0.8 and packet payload size (L_P) is fixed to 128 byte in this figure. As expected, as the R_{net} increases, the maximum normalized lifetimes for all types of error control schemes decrease for Mica2 and Telos. Among all network utilizing various error control schemes, the network using ARQ has the lowest lifetime for Mica2 and Telos. Since, during bad channel conditions, the higher number of retransmission causing higher transmission energy consumption. For all error control schemes, the lifetime of Telos outperforms the Mica2 by virtue of higher data rate and lower processing power. In fact, HARQ-II performs the best lifetime values for Mica2 while BCH(31,21,5) performs the best lifetime values for Telos because of lower processing power. Since, the lower processing power considerably decreases the decoding energy consumption. It is clear that since the only redundant bits transmitted in retransmission, HARQ-II achieves greater lifetime than that of HARQ-I. BCH(31,21,5) shows better performance compared to BCH(31,11,5) for lifetime maximization. Even if both are able to correct the same number of bits, their payload size is different in FEC block. The less payload size, the higher number of FEC block with redundant bits is causing excessive energy consumption in transmission. Furthermore, these redundant bits overload the battery of receiver nodes while decoding the data. Although BCH(31,11,5) and RS(15,11,2) have the same payload size, the BCH (31,11,5) provides higher error correction capabilities as well the higher redundant bits are increasing the energy consumption. In other words, BCH (31,11,5) has the larger FEC block length leads to more energy consumption. Therefore, the lifetime of RS(15,11,2) is higher than that of BCH(31,11,5).

The Fig. 3 presents the normalized network lifetime with respect to different number of packets (s) generated at each round in LOS environment. The figure is obtained when R_{net} and r is set to 10 m and 0.8, respectively. As the number of packets increase, the normalized maximum network lifetime decreases for both Mica2 and Telos. Since the greater number of packets increase the flows relaying on sensors in the network, the energy consumption of sensors increase. The Fig. 4 demonstrates the normalized network lifetime with respect to various desired application reliability rate (r) of the network. The analysis is performed when R_{net} is 10 m and L_P is 128 byte. As the desired reliability rate increases, the lifetime decreases. While trying to provide desired reliability rate, the routing path options for sensor nodes is restricted. Therefore, relaying on the same routing paths causes the battery of sensor nodes on the paths run out faster. For Telos motes, we see that RS(15,11,2) and ARQ schemes can not find any feasible solution where reliability rate is equal to 1.

Figs. 5 and 6 demonstrate the normalized lifetime of error control schemes with respect to different environment topographies for Mica2 and Telos, respectively. The network radius (R_{net}) is set 10 m and the application reliability is set 0.8 in these figures. Since path loss exponent of OBS (heavy clutter) is the highest, it has the least network lifetime among all environment topographies for both Mica2 and Telos. As the path loss exponent increases, SNR over the path decreases. In other words, the BER increases in harsh industrial environments, such as in OBS (heavy clutter) and ALL LSF environments. The increased BER does not change the lifetime order of error control schemes for Telos. However, BCH(31,11,5) becomes error control scheme which has the least lifetime in all environments harsher than LOS environments for Mica2. The reason is that BCH (31,11,5) has too much redundant bits. These excessive redundant bits cause more energy consumption for Mica with high processing power and low data rate.

The Table 5 illustrates the impact of ARQ, FEC, HARQ-I and HARQ-II schemes on industrial network lifetime where R_{net} increases from 10 m to 20 m for Mica2 and Telos motes. The evaluation is obtained by considering L_P as 128 byte and r as 0.8. It is clearly seen that indoor solar harvester scavenges more energy compared to others in industrial environments and hence, it has great potential to prolong lifetime

substantially. For instance, when R_{net} is 10 m vibration and thermal harvester increases lifetime approximately by %18 and %30, respectively whereas indoor solar harvester %46 for Mica2 with HARQ-II. As observed for Mica2, indoor solar harvester provides the maximum improvement to the network lifetime also for Telos. For instance, when R_{net} is 10 m vibration and thermal harvester increases lifetime approximately by %25 and %44, respectively whereas indoor solar harvester %71 for BCH(31,21,5).

5. Conclusions

In this paper, we presented the performance evaluations of the error control schemes (*i.e.*, ARQ, FEC and HARQ) and their impact on industrial WSNs' lifetime. The MIP framework is designed jointly using realistic channel model for industrial environments and energy dissipation models. Moreover, the impacts of vibration, thermal and indoor solar harvesting methods on network lifetime is investigated. The conclusions of this paper based on evaluations can be summarized as follows:

- Utilizing HARQ-II error control scheme for Mica2 at link layer outperforms the other error control schemes in terms of network lifetime, while providing desired application reliability rate. Since the lower processing power consumption of Telos nodes significantly decreases the decoding energy of FEC codes, BCH (31,21,5) scheme reaches the maximum lifetime.
- The maximum network lifetime of Telos is grater than that of Mica2 due to higher data rate and low processing power consumption of Telos. The higher data rate reduces the network overhead, hence prolongs the network lifetime greatly.
- Among the harvesters used in industrial environments, the network lifetime improvement of indoor solar harvester is considerably greater than others. The lifetime improvements achieved with indoor solar harvester is %46, %71 for Mica2 and Telos, respectively.

As a future work, the proposed MIP framework will be extended to examine the node level network for multimedia communication. In node level network, suitable error control scheme can be determined over each link in order to provide energy efficiency and link reliability for each transmission. In addition, cross-layer communication approaches and the impacts of different heterogeneous resources, such as network bandwidth and processing capacity, on overall network performance will be investigated to improve network lifetime and reliability.

Declaration of competing interest

The authors whose names are listed immediately below certify that they have NO affiliations with or involvement in any organization or entity with any financial interest (such as honoraria; educational grants; participation in speakers bureaus; membership, employment, consultancies, stock ownership, or other equity interest; and expert testimony or patent-licensing arrangements), or non-financial interest (such as personal or professional relationships, affiliations, knowledge or beliefs) in the subject matter or materials discussed in this manuscript.

References

[1] E. J. Colbert, A. Kott, Cyber-security of industrial control systems.
[2] Z.B. Celik, L. Babun, A.K. Sikder, H. Aksu, G. Tan, P. McDaniel, A.S. Uluagac, Sensitive information tracking in commodity IoT, 27th {USENIX} Security Symposium ({USENIX} Security 18), (2018), pp. 1687–1704.
[3] V.C. Gungor, G.P. Hancke, et al., Industrial wireless sensor networks: challenges, design principles, and technical approaches. IEEE Trans. Ind. Electron. 56 (10) (2009) 4258–4265.
[4] K.S. Low, W.N.N. Win, M.J. Er, Wireless sensor networks for industrial environments, Null, IEEE, 2005, pp. 271–276.
[5] A.K. Sikder, A. Acar, H. Aksu, A.S. Uluagac, K. Akkaya, M. Conti, IoT-enabled smart lighting systems for smart cities, 2018 IEEE 8th Annual Computing and Communication Workshop and Conference (CCWC), IEEE, 2018, pp. 639–645.
[6] A.S. Uluagac, C.P. Lee, R.A. Beyah, J.A. Copeland, Designing secure protocols for wireless sensor networks, International Conference on Wireless Algorithms, Systems, and Applications, Springer, 2008, pp. 503–514.
[7] K. Yu, M. Gidlund, J. Åkerberg, M. Bjorkman, Reliable and low latency transmission in industrial wireless sensor networks, Procedia Comput. Sci. 5 (2011) 866–873.
[8] M.C. Vuran, I.F. Akyildiz, Error control in wireless sensor networks: a cross layer analysis, IEEE/ACM Trans. Netw. 17 (4) (2009) 1186–1199.
[9] A. Nandi, S. Kundu, Energy level performance of error control schemes in WSN over rayleigh fading channel, Industrial Electronics and Applications (ISIEA), 2011 IEEE Symposium on, IEEE, 2011, pp. 194–199.
[10] M.R. Islam, Error correction codes in wireless sensor network: an energy aware approach, Int. J. Comput. Inf.Eng. 4 (1) (2010) 59–64.
[11] M.Y. Naderi, H.R. Rabiee, M. Khansari, M. Salehi, Error control for multimedia communications in wireless sensor networks: a comparative performance analysis, Ad Hoc Netw. 10 (6) (2012) 1028–1042.
[12] B. Sarvi, H.R. Rabiee, K. Mizanian, An adaptive cross-layer error control protocol for wireless multimedia sensor networks, Ad Hoc Netw. 56 (2017) 173–185.
[13] S.M. Razali, K. Mamat, N.S.K. Bashah, Implementation of hybrid ARQ (HARQ) error control algorithm for lifetime maximization and low overhead cdma wireless sensor network (WSN), Wireless Sensors (ICWiSE), 2016 IEEE Conference on, IEEE, 2016, pp. 71–76.
[14] F. Jalali, S. Khodadoustan, A. Ejlali, Error control schemes in solar energy harvesting wireless sensor networks, Communications and Information Technologies (ISCIT), 2012 International Symposium on, IEEE, 2012, pp. 979–984.
[15] M.K. Sharma, C.R. Murthy, Packet drop probability analysis of ARQ and HARQ-CCwith energy harvesting transmitters and receivers, Signal and Information Processing (GlobalSIP), 2014 IEEE Global Conference on, IEEE, 2014, pp. 148–152.
[16] H. Mahdavi-Doost, R.D. Yates, Hybrid ARQ in block-fading channels with an energy harvesting receiver, Information Theory (ISIT), 2015 IEEE International Symposium on, IEEE, 2015, pp. 1144–1148.
[17] A. Yadav, M. Goonewardena, W. Ajib, O.A. Dobre, H. Elbiaze, Energy management for energy harvesting wireless sensors with adaptive retransmission, IEEE Trans. Commun. 65 (12) (2017) 5487–5498.
[18] J. Jung, M. Kang, I. Yoon, D.K. Noh, Adaptive forward error correction scheme to improve data reliability in solar-powered wireless sensor networks, Information Science and Security (ICISS), 2016 International Conference on, IEEE, 2016, pp. 1–4.
[19] N. Tekin, V.C. Gungor, Lifetime analysis of error control schemes on wireless sensor networks in industrial environments, 2019 27th Signal Processing and Communications Applications Conference (SIU), IEEE, 2019.
[20] G. Gao, H. Zhang, L. Li, Performance evaluation of WSNs-based link quality estimation metrics for industrial environments, Advanced Technologies in Ad Hoc and Sensor Networks, Springer, 2014, pp. 69–79.
[21] M. Zuniga, B. Krishnamachari, Analyzing the transitional region in low power wireless links, Sensor and Ad Hoc Communications and Networks, 2004. IEEE SECON 2004. 2004 First Annual IEEE Communications Society Conference on, IEEE, 2004, pp. 517–526.
[22] A. Akbas, H.U. Yildiz, B. Tavli, S. Uludag, Joint optimization of transmission power level and packet size for WSN lifetime maximization, IEEE Sens. J. 16 (12) (2016) 5084–5094.
[23] M.C. Domingo, M.C. Vuran, Cross-layer analysis of error control in underwater wireless sensor networks, Comput. Commun. 35 (17) (2012) 2162–2172.
[24] S. Kurt, H.U. Yildiz, M. Yigit, B. Tavli, V.C. Gungor, Packet size optimization in wireless sensor networks for smart grid applications, IEEE Trans. Ind. Electron. 64 (3) (2017) 2392–2401.
[25] H.U. Yildiz, B. Tavli, H. Yanikomeroglu, Transmission power control for link-level handshaking in wireless sensor networks, IEEE Sens. J. 16 (2) (2016) 561–576.
[26] J.-S. Ahn, J.-H. Yoon, K.-W. Lee, Performance and energy consumption analysis of 802.11 with FEC codes over wireless sensor networks, J. Commun. Netw. 9 (3) (2007) 265–273.
[27] M.C. Vuran, I.F. Akyildiz, Cross-layer analysis of error control in wireless sensor networks, Sensor and Ad Hoc Communications and Networks, 2006. SECON'06. 2006 3rd Annual IEEE Communications Society on, 2 IEEE, 2006, pp. 585–594.
[28] J. Oueis, R. Stanica, F. Valois, Energy harvesting wireless sensor networks: from characterization to duty cycle dimensioning, Mobile Ad Hoc and Sensor Systems (MASS), 2016 IEEE 13th International Conference on, IEEE, 2016, pp. 183–191.
[29] N. Tekin, H.E. Erdem, V.C. Gungor, Analyzing lifetime of energy harvesting wireless multimedia sensor nodes in industrial environments, Comput. Stand. Interfaces 58 (2018) 109–117.
[30] K. Uchida, S. Takahashi, K. Harii, J. Ieda, W. Koshibae, K. Ando, S. Maekawa, E. Saitoh, Observation of the spin seebeck effect, Nature 455 (7214) (2008) 778.
[31] Mica2 Datasheet.
[32] J. Polastre, R. Szewczyk, D. Culler, Telos: enabling ultra-low power wireless research, Information Processing in Sensor Networks, 2005. IPSN 2005. Fourth International Symposium on, IEEE, 2005, pp. 364–369.
[33] V. Shnayder, M. Hempstead, B.-r. Chen, G.W. Allen, M. Welsh, Simulating the power consumption of large-scale sensor network applications, Proceedings of the 2nd international conference on Embedded networked sensor systems, ACM, 2004, pp. 188–200.
[34] Msp430 Datasheet.
[35] C. Eris, M. Saimler, V.C. Gungor, E. Fadel, I.F. Akyildiz, Lifetime analysis of wireless sensor nodes in different smart grid environments, Wirel. Netw. 20 (7) (2014) 2053–2062.
[36] K. Bicakci, I.E. Bagci, B. Tavli, Communication/computation tradeoffs for prolonging network lifetime in wireless sensor networks: the case of digital signatures, Inf. Sci. 188 (2012) 44–63.